

Simulating Continental Surface Waters: An Application to Holocene Northern Africa

MICHAEL T. COE

*IES Center for Climatic Research and Department of Atmospheric and Oceanic Sciences,
University of Wisconsin—Madison, Madison, Wisconsin*

(Manuscript received 31 January 1996, in final form 23 September 1996)

ABSTRACT

A model (SWAM) to predict surface waters (lakes and wetlands) on the scale of atmospheric general circulation models is developed. SWAM is based on a linear reservoir hydrologic model and is driven by runoff, precipitation, evaporation, topography, and water transport directions.

SWAM is applied to the modern climate using observed estimates of the hydrologic variables and a $5' \times 5'$ digital terrain model to represent topography. It simulates the surface water area of northern Africa (about 1% of the land area) in reasonable agreement with observed estimates (0.65%). A middle Holocene (6000 yr BP) simulation using the results of the GENESIS atmospheric general circulation model (AGCM) illustrates the sensitivity of the simulated surface waters to climatic changes and the model's utility as a diagnostic tool for AGCMs. SWAM and GENESIS capture the general pattern of climate change 6000 yr BP. There is an increase in the simulated surface water area from about 1% to about 3% of the land area, including an increase in the area of Lake Chad by about five times and extensive surface water throughout northern Mali, consistent with observed patterns of surface water change during the Holocene. Limitations in the modeling of surface waters appear to result from the relatively coarse resolution of global elevation data.

1. Introduction

Observations have shown that surface waters (lakes and wetlands) are an important component of the climate system (Carpenter 1984; Eichenlaub 1979; McCoy and Williams 1984; Benson and Thompson 1987), often contributing to the regional moisture budget through increased precipitation and often reducing the seasonal and diurnal temperature range. In addition, simulations have confirmed the importance of surface water in determining regional climate (Pitman 1991; Henderson-Sellers and Pitman 1992; Hostetler and Giorgi 1992; Bates et al. 1993; Hostetler et al. 1993; Hostetler et al. 1994).

Land-surface parameterizations, to be used in conjunction with atmospheric general circulation models (AGCMs), have recently been developed to include sub-grid-scale surface water (Pitman 1991; Henderson-Sellers and Pitman 1992; Bonan 1995). Results from global climate simulations have shown that including surface waters often improves the simulation with respect to observations (Kutzbach and Ziegler 1993; Bonan 1995).

However, parameterizing surface water in AGCMs

with fixed geographic lake locations is of limited use to climate change studies because the location of surface waters is not static. The maxima in the zonal mean surface water distribution are associated with the mean positions of the westerlies and the ITCZ, which correspond to maxima in storm track and tropical precipitation (Street-Perrott and Roberts 1983). Therefore, the location of the surface water maxima change through time in conjunction with shifts in the mean positions of the westerlies and the ITCZ (Street-Perrott and Roberts 1983; Harrison and Metcalfe 1985; Harrison and Dodson 1993; Harrison et al. 1993). For example, a dramatic increase in the number and size of lakes, wetlands, and river systems in northern Africa during the early to middle Holocene (e.g., Street and Grove 1979; Petit-Maire et al. 1993; Jolly et al. 1997) indicates a probable northward shift in the monsoon rains and mean position of the ITCZ. Therefore, for accurate climate change simulations, surface waters must be an interactive component of climate models.

This paper presents a model (SWAM) that predicts the distribution of surface waters given inputs of runoff, precipitation, evaporation, high-resolution topographic data, and water transport directions. The model has been applied to two climate regimes: 1) the modern observed climate and 2) a simulated middle Holocene climate (6000 yr BP). The focus of this study is on northern Africa, although the ultimate goal is to make predictions of surface waters for all continents.

Corresponding author address: Dr. Michael T. Coe, Center for Climatic Research, Institute for Environmental Studies, University of Wisconsin—Madison, 1225 West Dayton Street, Madison, WI 53706-1695.

E-mail: coe@phoebus.meteor.wisc.edu

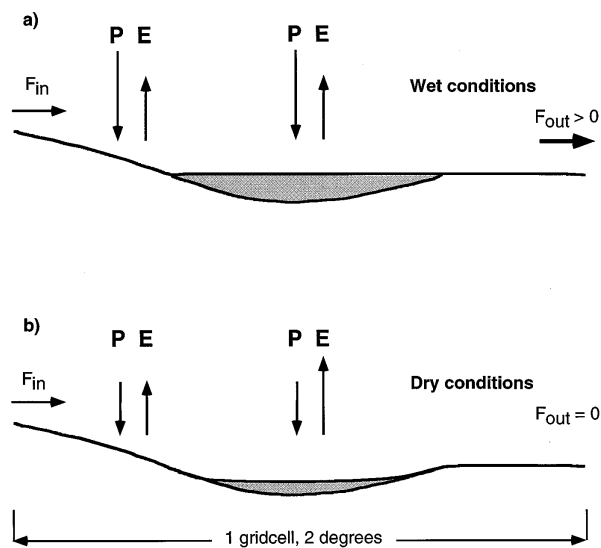


FIG. 1. Schematic diagram of a SWAM grid cell, showing surface water as a function of the transport of water (F_{in} , if any) from the upstream grid cell(s) and the precipitation and evaporation over the land and water fraction. The basin is filled according to the water volume available [shaded area; (a) wet and (b) dry conditions are shown]. Excess water (F_{out} , if any) is transported to the downstream grid cell.

2. Model description

SWAM calculates the area of surface waters as a function of both the volume of water present and the local topography (Fig. 1). The volume of water present is calculated at a resolution of $2^\circ \text{ lat} \times 2^\circ \text{ long}$ as the sum of the precipitation minus the evaporation ($P - E$) over the water and land-surface fractions and the transport of water from upstream grid cells. The transport of water from upstream grid cells is a function of the upstream moisture budget and a prescribed water transport direction (Fig. 2). The water volume (WV) present in a grid cell is then distributed onto a $5' \times 5'$ representation of the land surface. The high-resolution topography defines how WV is expressed on the surface by defining the shape of the basin (shallow or steep sided) and by defining the maximum fractional water area (MFWA) that can be accommodated in a $2^\circ \times 2^\circ$ grid cell. Any WV within a $2^\circ \times 2^\circ$ grid cell in excess of that required for MFWA is transported to the downstream grid cell. The calculation of the surface water area in SWAM, therefore, involves two steps: 1) determination of WV present in each of the $2^\circ \times 2^\circ$ grid cells and 2) conversion of the WV to fractional water area (FWA) on the $5' \times 5'$ representation of the land surface. Using two different resolutions within the model retains the influence of the high-resolution topography while calculating the water budget on the resolution of a climate model.

a. Topographic input

The Terrainbase $5' \times 5'$ (roughly $10 \text{ km} \times 10 \text{ km}$ at the equator and 1 m in the vertical) digital terrain

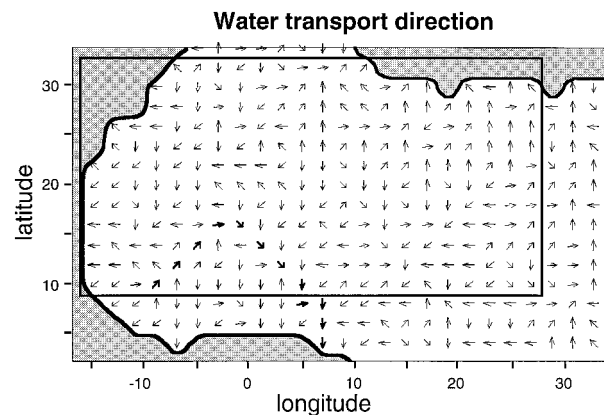


FIG. 2. Water transport directions prescribed from visual inspection of the Rand McNally *New International Atlas* (1989). Arrows represent the direction in which discharge is exported from a grid cell in SWAM. The Niger River has been highlighted as an example of a feature that appears on the $2^\circ \times 2^\circ$ scale of this model. The black box encloses the area for which averages and coefficients of correlation were calculated in this study.

model (DTM) from the National Oceanic and Atmospheric Administration National Geophysical Data Center was used to represent the land surface. This dataset is derived from interpretation of diverse sources of data including satellite and land-based data. The elevation in the DTM represents an estimate of the height for a given area but is not an actual measurement.

The maximum fractional water area is derived from Terrainbase for the $2^\circ \times 2^\circ$ grid of SWAM. MFWA is calculated in a manner similar to that used by MacMillan (1993) to define potholes in an Alberta farm field. An iterative search of the DTM defines all closed depressions in the landscape and their outlet heights. A potential water area (PWA; Fig. 3a) is defined as the area of a closed depression with an elevation equal to or lower than the outlet elevation. The MFWA for each $2^\circ \times 2^\circ$ grid cell is obtained by summing the PWA within each grid cell and dividing by the total area of the grid cell. Once defined, MFWA is invariant.

b. Linear reservoir model

Water flow is represented by a linear reservoir model (Huggins and Burney 1982), which has been shown to be reliable in addressing questions of large-scale hydrology. This approach has been used to investigate the relationship between climate and the surface area of closed lakes (Snyder and Langbein 1962; Szesztay 1974; Miffin and Wheat 1979; Street 1979; Street 1980; Servant and Servant-Vildary 1980; Bowler 1981; Street-Perrott and Harrison 1985; Street-Perrott and Perrott 1993). It has also been used to determine the timing and magnitude of discharge of the Amazon–Tocantins River basin (Vörösmarty et al. 1989) and the Zambezi River basin (Vörösmarty and Moore 1991; Vörösmarty et al. 1991) given monthly runoff distributions for the basins.

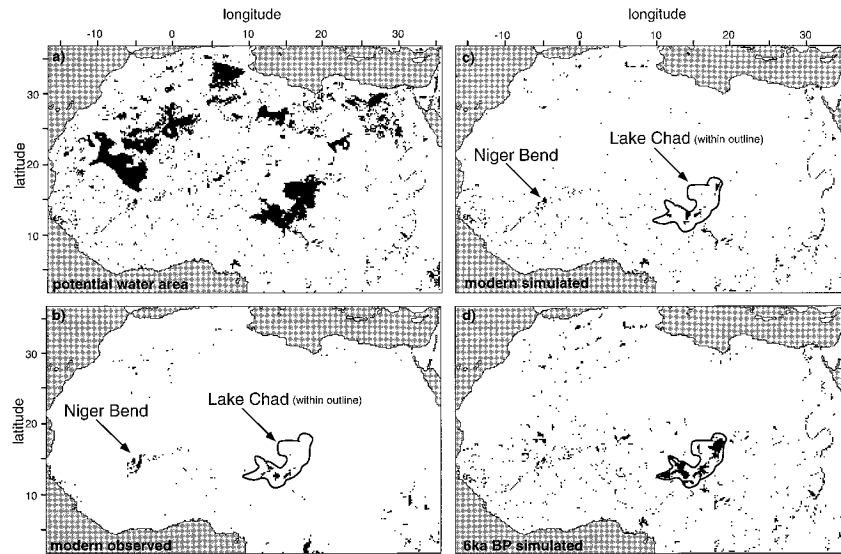


FIG. 3. Chart of the surface waters of northern Africa (shown in black) at the $5' \times 5'$ resolution of the model topography. (a) Simulated PWA derived from the $5' \times 5'$ Terrainbase digital terrain model. Black areas represent areas of surface water if runoff is unlimited. (b) Modern observations (Cogley 1991), provided at $1^\circ \times 1^\circ$ resolution and distributed into the $5' \times 5'$ Terrainbase DTM. (c) Modern epoch simulated using observed runoff and precipitation. (d) Middle Holocene simulated using differences between GENESIS 6 kyr BP and modern simulated runoff and precipitation added to modern observed values. The maximum possible area of Lake Chad is shown in the schematic outline of (b)–(d).

Additionally, it has been used as a diagnostic tool for comparing the magnitude and timing of AGCM simulated mean monthly runoff to observations (Miller et al. 1994; Marengo et al. 1994).

Each $2^\circ \times 2^\circ$ grid cell is considered to be a storage pool where the change with time of the water volume is represented by the following equation:

$$\frac{d(WV)}{dt} = R_b(1 - FWA) + (P_w - E_w)FWA + (\sum F_{in} - F_{out}) + (G_{in} - G_{out}) + F_c,$$

where FWA is the fractional water area in the grid cell; R_b is the grid cell land runoff (surface runoff + base flow); and P_w and E_w are the precipitation and evaporation over the water, respectively. Here, G_{in} and G_{out} are the groundwater fluxes into and out of the grid cell, and F_c is a flux correction included to maintain level water surfaces; F_{out} is the flux out of the grid cell, and $\sum F_{in}$ is the sum of the fluxes of water (F_{out}) from the upstream cells.

The net transport by groundwater ($G_{in} - G_{out}$) is considered to be zero in this study. A scale analysis suggests why this is possible (Cogley 1989). In general, transport of water to the groundwater reservoir from the runoff reservoir is positive (directed downward) on plateaus and hill slopes, and negative in valleys, lakes, and wetlands. Surface topographic heterogeneity generally dictates that net transport between the groundwater and runoff reservoirs approaches zero for spatial scales greater than hundreds of square kilometers ($\ll 1$ SWAM grid cell). Therefore, for ($G_{in} - G_{out}$) to be other than

zero, the groundwater head between grid cells must differ. However, since groundwater flow rates are on the order of \approx tens of meters per year, the timescale of flow would be millennia or longer and is, therefore, a result of a past climate state. Transport of this nature may occur in northern Africa, but it cannot be modeled in this study.

Here, F_{out} depends upon the existence of water in excess of the maximum water volume (MWV; if any) $WV - MWV$ and a timescale defined by the ratio of the flow rate (u) to the downstream distance (D):

$$F_{out} = \max[(WV - MWV), 0](u/D),$$

where MWV is the volume that corresponds to $FWA = MFWA$. The flow rate u depends upon a ratio of the downstream gradient (ic) and a reference gradient (io ; Miller et al. 1994):

$$u = 0.35 \times (ic/io)^{0.5},$$

where io is set to 5×10^{-5} (Miller et al. 1994). This approximation of the flow rate is adequate for this study since the flow rate has no effect on the equilibrium surface water area.

Routing of F_{out} requires knowledge of the water transport directions. The water transport directions at the $2^\circ \times 2^\circ$ resolution are prescribed (Fig. 2) from visual inspection of the Rand McNally *The New International Atlas* (1989) (as in Vörösmarty et al. 1989; Miller et al. 1994). For each grid cell, a predominant direction of transport is determined by examining the network of

streams. Where a stream network is not discernible, the transport direction is determined from the topographic features and elevations.

FWA is calculated for each grid cell by distributing WV directly onto the $5' \times 5'$ land surface starting with the lowest elevation that corresponds to PWA within a grid cell and proceeding to other PWAs with higher elevations as necessary. FWA may be a value from 0 km² (WV = 0) to MFWA (WV = MWV).

Here, F_c accounts for the movement of water in bodies larger than the $2^\circ \times 2^\circ$ grid cell of the water budget component of the model. If no flux correction is made, a large water body could have an uneven surface owing to the different water mass balances of adjacent cells; F_c allows for the transfer of water counter to the prescribed water transport direction, where necessary, to maintain a level surface. The F_c is calculated where there is a downstream water surface elevation (WE_d) in excess of both the local water surface elevation (WE_L) and the local outlet elevation (O_L). In other words, the elevation of the downstream water surface (WE_d) is compared to the local water elevation (WE_L) and the elevation of land-surface communication between the two grid cells (O_L). If the downstream water elevation exceeds the local water-surface elevation and the outlet elevation, then F_c shifts some of the water volume from downstream to the local grid cell in the following manner:

$$F_c = \int_{O_L}^{WE_d} A(z) dz \times 0.1.$$

The factor of 0.1 approximates $1/n$, where n is the maximum number of grid cells (≈ 10) constituting a large water surface in northern Africa; $A(z)$ is the surface area at each elevation (z). When applied over several iterations, the flux correction F_c causes large water surfaces to converge to a uniform level.

Starting with WV and FWA = 0 and forcing the model with mean annual observed values of R_p , P_w , and E_w converted to daily values, SWAM solves for $d(WV)/dt$ until equilibrium is reached [$d(WV)/dt$ is small with no trend]. It was found through experimentation that model convergence required a time step of several days. For this study, a time step of 1 day was used. A 1-day time step has the additional advantage that the model can be used with seasonally and daily varying input in future studies. The resultant WV and corresponding FWA represent the water volume and fractional surface water area in equilibrium with the prescribed mean annual climate.

3. Modern climate

A simulation was performed with estimates of the modern mean annual runoff and surface water precipitation and evaporation to determine the ability of the model to produce the modern perennial surface water distribution of northern Africa. Simulation of the mean

annual surface water area was chosen for this study (rather than monthly or seasonal) because no seasonal or monthly datasets of runoff or observed surface water area were available for forcing the model or for comparison with the model results. Discussion of the results will be limited to the region 10° to 34° N, 16° W to 28° E (Fig. 2).

The surface runoff used was a digitized version (Cogley 1989) of the UNESCO (1978) mean annual river runoff interpolated to $2^\circ \times 2^\circ$. The runoff dataset represents the mean annual surface flux of water at each grid cell. Mean annual land precipitation values derived from Legates and Willmott (1990) were used as the surface water precipitation. All values were converted to daily rates.

Evaporation from the surface water is calculated using a linked system of equations as described in Parkinson and Washington (1979); see the appendix for details. This simple calculation adequately describes the surface water characteristics in northern Africa. For example, the calculated annual average water temperature (28° C) and evaporation (2100 mm yr^{-1}) from the simulated Lake Chad are within 10% of the calculated estimates of 26.5° C and 2200 mm yr^{-1} of Tetzlaff and Adams (1983).

The estimates of the surface areas of perennial lakes, wetlands, and salt marshes of Cogley (1991) are used for comparison with the simulated surface water area. Cogley's estimates are derived from visual inspection of maps with a scale of 1:1 000 000. He estimates the root-mean-square error of measurement in the individual datasets to be a few percent, not including errors on the maps themselves. Cogley concludes that these measurements are accurate at resolutions of $4^\circ \times 4^\circ$ or coarser. For comparison purposes, the salt marsh data here have been masked to remove coastal marshes, which are a function of sea level and not the local moisture budget. In addition, the lake, wetland, and masked salt marsh datasets have been summed to produce a fractional surface water area dataset (referred to as OBS in the text).

The modern mean annual surface water simulation is in reasonable agreement with the observations. The model simulates water as occupying about 1% of the land area of northern Africa (Table 1 and Fig. 4), compared to about 0.65% for OBS. The coefficient of correlation between the simulated and observed surface water for the $66 \ 4^\circ \times 4^\circ$ grid cells constituting northern Africa is 0.77 (Table 1).

Surface water is a significant fraction of the land area in only two regions of northern Africa today (Fig. 3b): Lake Chad (10° – 18° N, 10° – 20° E) and the bend of the Niger River (12° to 16° N, 6° to 2° W). The total surface water area simulated for the Lake Chad basin is about 28 000 km², which is somewhat larger than the 22 000 km² of OBS and the bounds of historical fluctuations of Lake Chad (17 000 to 25 000 km²; Beadle 1974). The discrepancy between the observed and simulated

TABLE 1. Comparison of observed and simulated modern surface water area averaged over North Africa (10° – 34° N; 16° W– 28° E). The area is expressed as the percentage of the total land area. Correlation refers to the coefficient of correlation between the simulated and observed surface water for the $66\ 4^{\circ} \times 4^{\circ}$ grid cells in the area of interest. Three simulations are shown: SWAM is derived from the mean annual runoff and precipitation, SWAM– is derived from subtraction of the estimates of error from the annual mean, and SWAM+ is derived from addition of the estimates of error to the annual mean.

	% area	Correlation
OBS	0.65	*
SWAM	0.97	0.77
SWAM–	0.80	0.79
SWAM+	1.19	0.72

area of Lake Chad suggests that the model overestimates the net water budget of the Chad Basin. The shape of the simulated lake differs from the observed (Figs. 3b,c) because the DTM used in the model is unable to differentiate between the upper basin where the modern lake is located and the lower Bodélé depression to the northeast. As a result, the model allows a large share of the lake to flow into the Bodélé depression.

The Niger bend system is accurately placed by the model, but the area is too small—about 11 000 km² compared to about 24 000 km² for OBS. Comparison of the simulated area (Fig. 3c) with the potential water area (Fig. 3a) indicates that the model does not simulate the potential for surface water area greater than this at the Niger bend. The Niger bend is a system of small interconnected wetlands and lakes fed by the seasonal flooding of the Niger River (Beadle 1974; Petit-Maire et al. 1988). Many of these depressions are smaller than the $5' \times 5'$ resolution of the DTM and therefore escape detection by SWAM.

To the southeast of Lake Chad, the model simulates considerable surface water, which is associated with the Chari River and not supported by OBS. However, the Rand McNally *New International Atlas* (1989) depicts an extensive area of wetlands in this region, and there are large perennial wetlands associated with the inland delta of the Chari River (Durand 1982).

SWAM simulates many small water bodies (<5% of a $2^{\circ} \times 2^{\circ}$ grid cell area) in the southern humid region that are not supported by OBS (Figs. 3b,c). This is a result of the coarse resolution of the DTM, which often results in river valleys being depicted as small interconnected pools.

Two additional simulations were made to provide an estimate of the sensitivity of the modern surface water simulation to error in the input values. In these simulations, the modern runoff and precipitation are modified by adding or subtracting the estimates of error given in Cogley (1989; generally about $\pm 15\%$, but much greater in arid regions) from the runoff and precipitation values of each grid cell. The results of this analysis suggest that the average simulated modern surface water area is not particularly sensitive to errors in the estimated

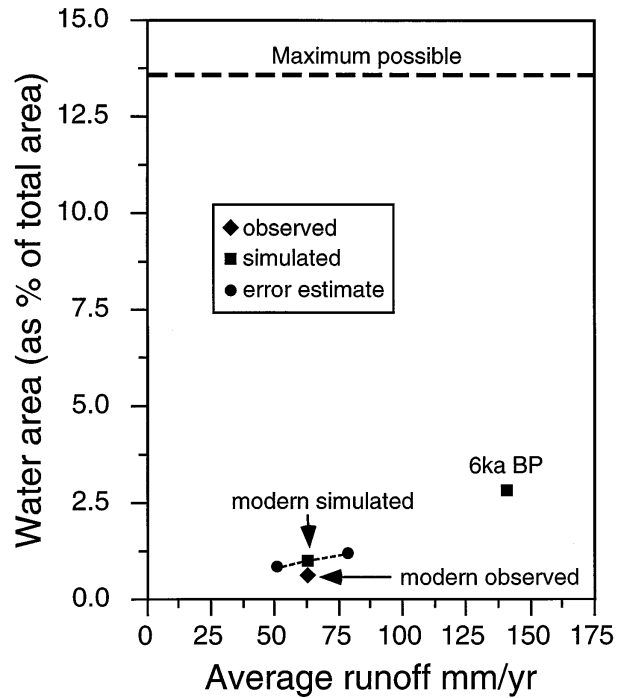


FIG. 4. Surface water area plotted against the area average runoff for observations (diamond) and modern and middle Holocene simulations (squares). Values are averaged over northern Africa (10° to 34° N, 16° W to 28° E; Fig. 2). The modern observed value represents an estimate of lakes, wetlands, and inland salt marshes by Cogley (1991). Maximum possible represents the maximum fractional water area that SWAM can simulate and corresponds to unlimited runoff. The modern simulation is derived from mean annual observed runoff (Cogley 1989) and precipitation (Legates and Willmott 1990). Estimates of error were used to infer the range of possible modern simulated surface water area, shown as dots. 6 kyr BP represents the results of forcing SWAM with observed runoff and precipitation plus the difference between 6kyr BP and modern simulations of runoff and precipitation on the GENESIS GCM version 1.02.

runoff and precipitation values (Table 1 and Fig. 4). Subtracting an amount equal to the estimate of error from each grid cell results in a decrease in the average runoff by about 20%, while the simulated surface water area decreases to about 0.80% from 0.97% of the total area. Similarly, addition of the error estimate increases the runoff by about 25% and increases the surface water area from 0.97% to 1.19%. Lake Chad is the only large surface water area to show sensitivity to these changes, with a simulated area of 19 000 and 37 000 km² for the subtraction and addition simulations, respectively.

4. Sensitivity to climate change: An application to a paleoclimate simulation

Lake levels in northern Africa were higher than at present between 10 000 and 5 000 yr BP (Fig. 5). Much of the Sahel and the now hyperarid core of the Sahara Desert was studded with river systems and small lakes (Street and Grove 1976; Street and Grove 1979; Petit-Maire and Riser 1981; Fontes et al. 1985; Lézine 1986;

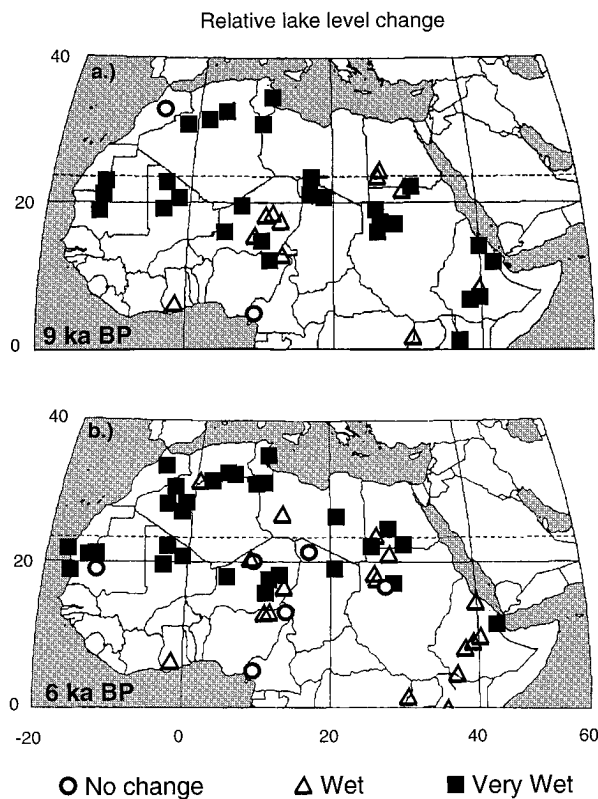


FIG. 5. Chart of the difference in lake status from the modern epoch for (a) 9000 ^{14}C yr BP and (b) 6000 ^{14}C yr BP adapted from Jolly et al. (1977). Very wet (square) refers to lakes that were much higher than present, wet (triangle) refers to lakes that were higher than present, and circles indicate no change.

Petit-Maire et al. 1987; Pachur and Kröppelin 1987; Haynes 1987; Haynes et al. 1989; Petit-Maire and Kröppelin 1991; Street-Perrott and Perrott 1993). Perennial freshwater lakes and wetlands associated with the inland delta of the Niger River constituted a large portion of the landscape of northern Mali (Petit-Maire et al. 1988; Street-Perrott et al. 1990). Observations also indicate that Lake Chad may have had a surface area of greater than 350 000 km^2 during the early and middle Holocene (Schneider 1967; Pias 1970).

General circulation model simulations indicate that the increased surface water in northern Africa was primarily caused by changes in the earth's orbital parameters. These orbital changes lead to an increased amplitude of the seasonal cycle of solar radiation and a strengthening and farther northward penetration of the summer monsoon (Kutzbach 1981). Observations suggest that the monsoon front may have penetrated 5° or more farther north during the middle Holocene than it does today (Butzer 1967; Street and Grove 1976; Fontes et al. 1985; Haynes et al. 1987; Petit-Maire et al. 1987; Lézine 1989; Lézine and Casanova 1989; Street-Perrott et al. 1990; Petit-Maire and Kröppelin 1991; Street-Perrott and Perrott 1993).

As an illustration of the sensitivity of SWAM to climate changes of this nature, the model was forced with estimates of runoff and surface water precipitation for 6 kyr BP. The 6 kyr BP runoff and precipitation were created for SWAM by adding the differences between 6 kyr BP and modern runoff and precipitation simulated by Foley (1994) on the National Center for Atmospheric Research GENESIS version 1.02 (Thompson and Polard 1995) to the modern observed values.

The boundary conditions of the modern and 6 kyr BP simulations on GENESIS differ only in the prescribed orbital parameters: eccentricity from 0.0167 (modern) to 0.0187 (6 kyr BP), axial tilt from 23.44° (modern) to 24.11° (6 kyr BP), and date of perihelion from January (modern) to mid-September (6 kyr BP). The change of the date of perihelion increases the amplitude of the seasonal cycle of solar radiation by about 5% in the Northern Hemisphere. The change in the amplitude of the seasonal solar radiation results in an increased summer land-ocean temperature and pressure contrast, increased moisture convergence, and increased precipitation and $P - E$ over northern Africa. The differences between the modern and 6 kyr BP results are consistent with previous AGCM simulations for the middle Holocene (Kutzbach 1981; Kutzbach and Otto-Bliesner 1982). A complete description of the GENESIS AGCM results can be found in Foley (1994).

The addition of the simulated differences to the modern observed values results in increased runoff (Figs. 6a,b) and precipitation (not shown but similar pattern to the runoff) across the Sahel north of about 10°N . The surface water evaporation per unit area in northern Africa was probably similar to the modern epoch during the early to middle Holocene (Kutzbach 1980) and therefore was unchanged from the modern epoch in the 6 kyr BP experiment.

The modern surface topography and prescribed water transport directions (Fig. 2) were used for the 6 kyr BP experiment. Changes in local topography and water transport direction have occurred during the Holocene in many of the lake basins through wind erosion of lake sediments (Petit-Maire 1986; S. Harrison 1996, personal communication). However, the scale of these changes is probably smaller than can be realistically resolved by the DTM or by the $2^\circ \times 2^\circ$ prescribed water transport directions.

The effect of the changes of the simulated middle Holocene monsoon is clearly expressed in the SWAM surface water simulations. There is an increase in the total surface water area of northern Africa from about 1% of the area in the modern simulation to about 3% with the added 6 kyr BP forcing (Table 2, and Figs. 3 and 4). Lake Chad is simulated to have a surface area of about 130 000 km^2 in the 6 kyr BP experiment (Table 2, and Fig. 3d). This is about five times the simulated modern surface water area but considerably less than the early to middle Holocene estimate of about 330 000 km^2 (Schneider 1967; Pias 1970). The surface water to

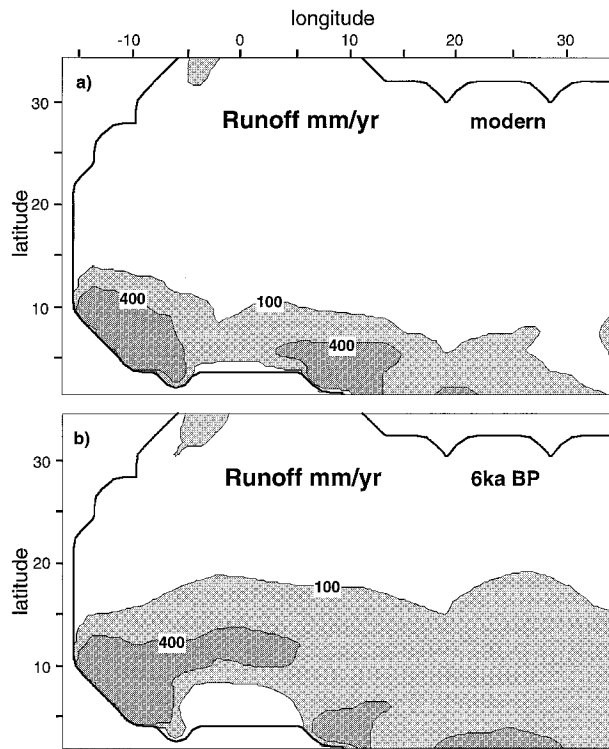


FIG. 6. Modern runoff and runoff 6 kyr BP in mm yr^{-1} for the two SWAM simulations. (a) Modern mean annual runoff. (b) Middle Holocene runoff derived by adding differences between GENESIS 6 kyr BP and modern simulated runoff to modern observed values. The 100 (light gray) and 400 (dark gray) mm yr^{-1} contours are shown.

the north of the Niger bend (16° and 20°N , 6° and 2°W) is simulated to expand to 16 000 km^2 in the 6 kyr BP experiment, which is much greater than the approximately 2000 km^2 in the modern simulation but less than the approximately 57 000 km^2 estimated (Street-Perrott et al. 1990; Petit-Maire et al. 1988). SWAM simulates the potential for 350 000 km^2 of surface water for Lake Chad and 85 000 km^2 north of the Niger bend (Table 2). Therefore, the fact that the simulated surface waters are much less than the observational estimates can be attributed to the simulated precipitation and runoff and not to the constraints of the topography.

Only small areas of surface water (about 1%–5% of the $2^{\circ} \times 2^{\circ}$ grid cells) are simulated over the rest of Africa south of about 20°N . This is in general agreement with the field evidence of small scattered lakes throughout the Sahel and southern Sahara, although the simulated surface waters are perhaps not as far north in the southern Sahara as observations would suggest (to approximately 23°N ; Street and Grove 1979). There is also an increase in the simulated surface water area (about 2%–9% of the grid cell area) in northwestern Africa, consistent with observations (Fontes et al. 1985; Petit-Maire et al. 1993).

SWAM simulates no increase in the surface water area nor any potential for surface water in northern Su-

dan ($\approx 17^{\circ}\text{N}$, 23° – 27°E ; Fig. 3), where observations suggest that small lakes and wetlands may have covered as much as 20 000 km^2 during the early to middle Holocene (Pachur and Hoelzmann 1991). The model fails to simulate the potential for surface water in this region, probably because the individual basins are smaller than the resolution of the DTM.

	% Total	Lake Chad	N Niger
MOD	1	28 000	2 000
6 kyr BP	3	130 000	16 000
EST	*	330 000	57 000
PWA	14	350 000	85 000

The results of the 6 kyr BP experiment indicate a large sensitivity to changes in the strength of the monsoon. However, the results also show that GENESIS version 1.02 probably underestimates the strength of the 6 kyr BP monsoon since the resultant surface waters are considerably less than those observed. This illustrates the utility of SWAM as a tool for diagnosing the accuracy of climate simulations on AGCMs.

The results of the 6 kyr BP experiment indicate a large sensitivity to changes in the strength of the monsoon. However, the results also show that GENESIS version 1.02 probably underestimates the strength of the 6 kyr BP monsoon since the resultant surface waters are considerably less than those observed. This illustrates the utility of SWAM as a tool for diagnosing the accuracy of climate simulations on AGCMs.

5. Conclusions

Observations and numerical simulations indicate that inland surface waters are a potentially important and dynamic component of the climate system. Until recently, surface waters have been neglected in global climate simulations. The model presented here is a first attempt at developing a relatively simple and accurate means of predicting surface water area at the resolution of AGCMs, from estimates of runoff, precipitation, evaporation, topography, and water transport directions.

A similar methodology can be used for the global simulation of surface waters for modern and climate change experiments (past and future) with topographic datasets currently (or soon to be) available. SWAM-derived estimates of surface water can also be used as a tool for diagnosing the accuracy of past and present climate simulations.

The limitations on accurately simulating inland surface waters are largely a result of the coarse resolution of DTMs. The coarse resolution results in a variety of problems, including 1) underestimation of the potential water area through a failure to identify areas smaller than the resolution of the DTM (e.g., the Niger bend), 2) overestimation of the potential surface water area in river valleys, and 3) incorrect spatial distribution of the

surface water in a large lake through errors in the definition of the lake basin topography (e.g., the modern Lake Chad basin). Finer-resolution DTMs, such as the EROS Data Center 3 arc second global DTM, are being made available and should improve the accuracy of large-scale surface water simulation.

Acknowledgments. I wish to thank John Kutzbach and Jon Foley for their insight and guidance throughout this project. In addition, I wish to thank the staff of the Center for Climatic Research at the University of Wisconsin—Madison, especially Pat Behling and Rich Selin, for helping with data management and figures. Steve Vavrus provided a wealth of information on the thermal properties of lakes. Sandy Harrison and an anonymous reviewer provided valuable suggestions for improvement of this manuscript.

This project was completed at the Center for Climatic Research of the Institute for Environmental Studies at the University of Wisconsin—Madison with National Science Foundation support from Grant ATM93-18973. The Terrainbase DTM was provided by the National Geophysical Data Center and World Data Center—A for Solid Earth Geophysics.

APPENDIX

Calculation of the Surface Water Evaporation

Evaporation from the surface water is calculated using a linked system of equations based on those described in Parkinson and Washington (1979). Starting with an initial guess for the surface water temperature (T_w), consistent values of evaporation, sensible heat, and longwave radiation are obtained by solving the surface energy budget equation for T_w ,

$$\Delta T_w = [\Delta t / (C_w Z)] [S(1 - \alpha) + (1^\downarrow - 1^\uparrow) - H - \lambda E],$$

where S is the incoming solar radiation, α is the surface albedo, $1^\downarrow - 1^\uparrow$ is the net longwave radiation at the surface, H is the sensible heat flux, λ is the latent heat of vaporization, E is the evaporation, Δt is the time step of 1 day (86 400 s), C_w is the heat capacity of water ($4.186 \times 10^6 \text{ J m}^{-3} \text{ K}^{-1}$), and Z is the water depth (10 m).

Here, $S(1 - \alpha)$ and 1^\downarrow are derived from the $2^\circ \times 2^\circ$ global simulation by Levis et al. (1996) using the LSX land surface model (Pollard and Thompson 1995). A complete description of the LSX modern simulation and comparison of results with observations can be found in Levis et al. (1996). The monthly average values of $S(1 - \alpha)$ and 1^\downarrow are averaged annually and converted to daily values for use in SWAM.

Here, 1^\uparrow is calculated from the radiative temperature (σT_w^4), and H and E are determined from the standard bulk aerodynamic formulas

$$H = \rho C_p C_h V (T_a - T_w)$$

and

$$\lambda E = \rho \lambda C_h V (q_a - q_w).$$

Air density ρ is set at 1.275 kg m^{-3} (Ebert and Curry 1993). The specific heat of air C_p is set at the dry air value of $1005 \text{ J kg}^{-1} \text{ K}^{-1}$. Here, C_h is a transfer coefficient taken from Ebert and Curry (1993); V is the annual average wind speed derived from output of the GENESIS AGCM (Pollard and Thompson 1995) with a minimum value set to 3 m s^{-1} ; T_a is the mean annual air temperature derived from the data of Leemans and Cramer (1990); and q_a and q_w are the atmospheric and near-surface specific humidity, respectively. The formulas for the q 's are

$$q_w \approx (\varepsilon e_w) / p$$

and

$$q_a = (\text{rh}/100.) \times q_w,$$

where $\varepsilon = 0.622$ is the ratio of the molecular weight of water vapor to that of dry air (Wallace and Hobbs 1977), and surface pressure p is a constant value of 101 400 Pa. Saturation vapor pressure e_w is determined from the Clausius–Clapeyron equation (Wallace and Hobbs 1977) using T_w . The mean annual relative humidity rh is derived from the Worldwide Airfield Summaries dataset (World WeatherDisc 1994; see Levis et al. 1996 for details).

REFERENCES

- Bates, G. T., F. Giorgi, and S. W. Hostetler, 1993: Toward the simulation of the effects of the Great Lakes on climate. *Mon. Wea. Rev.*, **121**, 1373–1387.
- Beadle, L. C., 1974: *The Inland Water of Tropical Africa: An Introduction to Tropical Limnology*. Longman, 365 pp.
- Benson, L. V., and R. S. Thompson, 1987: The physical record of lakes in the Great Basin. *North America and Adjacent Oceans During the Last Deglaciation*, W. F. Ruddiman and H. E. Wright, Eds., Geological Society of America, 241–260.
- Bonan, G. B., 1995: Sensitivity of a GCM to inclusion of inland water surfaces. *J. Climate*, **8**, 2691–2704.
- Bowler, J. M., 1981: Australian salt lakes: A paleohydrological approach. *Hydrobiologia*, **82**, 431–444.
- Butzer, K. W., 1967: Climatic change in the arid zones of Africa during early to mid-Holocene times. *Proc. of Symp. on World Climate from 8000 to 0 B.C.*, London, United Kingdom, Royal Meteorological Society, 72–83.
- Carpenter, D. M., 1984: An introduction to Great Salt Lake effect snowfall. *Problems of and Prospects for Predicting Great Salt Lake Levels*, P. A. Kay and H. F. Diaz, Eds., Center Public Affairs Administration, University of Utah, 155–165.
- Cogley, J. G., 1989: Runoff from the world's landmasses: Amounts and uncertainties at 2-degree resolution. Trent Climate Note 89-3, 25 pp. [Available from Dept. of Geography, Trent University, Peterborough, ON K9J 7B8, Canada.]
- , 1991: GGHYDRO—Global Hydrological Data Release 2.0. Trent Climate Note 91-1, 12 pp. [Available from Dept. of Geography, Trent University, Peterborough, ON K9J 7B8, Canada.]
- Durand, A., 1982: Oscillations of Lake Chad over the past 50,000 years: New data and new hypothesis. *Palaeogeogr., Palaeoclimatol., Palaeoecol.*, **39**, 37–53.

- Ebert, E. E., and J. A. Curry, 1993: An intermediate one-dimensional thermodynamic sea ice model for investigating ice-atmosphere interactions. *J. Geophys. Res.*, **98**(C), 10 085–10 109.
- Eichenlaub, V. L., 1979: *Weather and Climate of the Great Lakes Region*. University of Notre Dame Press, 335 pp.
- Foley, J. A., 1994: The sensitivity of the terrestrial biosphere to climatic change: A simulation of the middle Holocene. *Global Biogeochem. Cycle*, **8**, 505–525.
- Fontes, J. C., F. Gasse, Y. Callot, J.-C. Plaziat, P. Carbonel, P. A. Dupeuple, and I. Kaczmarzka, 1985: Freshwater to marine-like environment from Holocene lakes in northern Sahara. *Nature*, **317**, 608–610.
- Harrison, S. P., and S. E. Metcalfe, 1985: Variations in lake levels during the Holocene in North America: An indicator of changes in the atmospheric circulation patterns. *Geogr. Phys. Quat.*, **39**, 141–150.
- , and J. Dodson, 1993: Climates of Australia and New Guinea since 18,000 yr BP. *Global Climates Since the Last Glacial Maximum*, H. E. Wright Jr., J. E. Kutzbach, P. J. T. Webb III, F. A. Street-Perrott, W. F. Ruddiman, and P. J. Bartlein, Eds., University of Minnesota Press, 265–293.
- , C. I. Prentice, and J. Guiot, 1993: Climatic control on lake-level changes in Europe. *Climate Dyn.*, **8**, 189–200.
- Haynes, C. V., Jr., 1987: Holocene migration rates of the Sudano-Saharan wetting front, Arba'in desert, eastern Sahara. *Prehistory of Arid North Africa*, A. H. Close, Ed., Southern Methodist University Press, 69–84.
- , C. H. Eyles, L. A. Pavlish, J. C. Ritchie, and M. Rybak, 1989: Holocene palaeoecology of the eastern Sahara; Selima Oasis. *Quat. Sci. Rev.*, **8**, 109–136.
- Henderson-Sellers, A., and A. J. Pitman, 1992: Land-surface schemes for future climate models: Specification, aggregation, and heterogeneity. *J. Geophys. Res.*, **97**(D), 2687–2696.
- Hostetler, S. W., and F. Giorgi, 1992: Use of a regional atmospheric model to simulate lake-atmosphere feedbacks associated with Pleistocene lakes Lahontan and Bonneville. *Climate Dyn.*, **7**, 39–44.
- , G. T. Bates, and F. Giorgi, 1993: Interactive coupling of a lake thermal model with a regional climate model. *J. Geophys. Res.*, **98**, 5045–5052.
- , F. Giorgi, G. T. Bates, and P. J. Bartlein, 1994: Lake-atmosphere feedbacks associated with paleolakes Bonneville and Lahontan. *Science*, **263**, 665–668.
- Huggins, L. F., and J. R. Burney, 1982: Surface runoff, storage, and routing. *Hydrologic Modeling of Small Watersheds*, C. T. Haan, Ed., American Society of Agricultural Engineering, 165–229.
- Jolly, D., S. P. Harrison, B. Damnati, and R. Bonnefille, 1997: Simulated climate and biomes of Africa during the late Quaternary: Comparison with pollen and lake status data. *Quat. Sci. Rev.*, in press.
- Kutzbach, J. E., 1980: Estimates of past climate of paleolake Chad, North Africa, based on a hydrological energy-balance model. *Quat. Res.*, **14**, 210–223.
- , 1981: Monsoon climate of the early Holocene: Climate experiment with the earth's orbital parameters for 9000 years ago. *Science*, **214**, 59–61.
- , and B. Otto-Bliesner, 1982: The sensitivity of the African-Asian monsoon climate to orbital parameter changes for 9000 years B.P. in a low resolution general circulation model. *J. Atmos. Sci.*, **39**, 1177–1188.
- , and A. M. Ziegler, 1993: Simulation of late Permian climate and biome with an atmosphere-ocean model: Comparisons with observations. *Philos. Trans. Roy. Soc. London, Ser. B*, **341**, 327–340.
- Leemans, R., and W. P. Cramer, 1990: The IIASA database for mean monthly values of temperature, precipitation, and cloudiness on a global terrestrial grid. IIASA Working Paper WP-90-41, 62 pp.
- Legates, D. R., and C. J. Willmott, 1990: Mean seasonal and spatial variability in gauge-corrected, global precipitation. *Int. J. Climatol.*, **10**, 111–127.
- Levis, S., M. T. Coe, and J. A. Foley, 1996: Hydrologic budget of a land surface model: A global application. *J. Geophys. Res.*, **101D**, 16 921–16 930.
- Lézine, A.-M., 1986: Environnement et paléoenvironnement des nîayes depuis 12,000 BP. *Changements Globaux en Afrique Durant le Quaternaire: Passé-Présent-Futur* (in French), H. Faure, L. Faure, and E. S. Diop, Eds., Editions de l'ORSTOM, 261–263.
- , 1989: Late Quaternary vegetation and climate of the Sahel. *Quat. Res.*, **32**, 317–334.
- , and J. Casanova, 1989: Pollen and hydrological evidence for the interpretation of past climates in tropical West Africa during the Holocene. *Quat. Sci. Rev.*, **8**, 45–55.
- MacMillan, R. A., 1993: Measuring and modelling depression storage and ephemeral ponding at a farm scale in Alberta, Canada. Ph.D. dissertation, University of Edinburgh.
- Marengo, J. A., J. R. Miller, G. L. Russell, C. E. Rosenzweig, and F. Abramopoulos, 1994: Calculations of river runoff in the GISS GCM: Impact of a new land-surface parameterization and river routing model on the hydrology of the Amazon River. *Climate Dyn.*, **10**, 349–361.
- McCoy, W. D., and L. D. Williams, 1984: Application of an energy-balance model to the late Pleistocene Little Canyon glacier with implications regarding the paleohydrology of Lake Bonneville. *Problems of and Prospects for Predicting Great Salt Lake Levels*, P. A. Kay and H. F. Diaz, Eds., Center Public Affairs Administration, University of Utah, 40–53.
- Miffilin, M. D., and M. M. Wheat, 1979: Pluvial lakes and estimated pluvial climates of Nevada. *Nev. Bur. Mines Geol. Bull.*, **94**, 1–57.
- Miller, J., G. Russell, and G. Caliri, 1994: Continental-scale river flow in climate models. *J. Climate*, **7**, 914–928.
- Pachur, H.-J., and S. Kröppelin, 1987: Wadi Howar: Paleoclimatic evidence from an extinct river system in the southeastern Sahara. *Science*, **237**, 298–300.
- , and P. Hoelzmann, 1991: Paleoclimatic implications of late Quaternary lacustrine sediments in western Nubia, Sudan. *Quat. Res.*, **36**, 257–276.
- Parkinson, C. L., and W. M. Washington, 1979: A large-scale numerical model of sea ice. *J. Geophys. Res.*, **84**(C), 311–337.
- Petit-Maire, N., 1986: Paleoclimates in the Sahara of Mali. *Episodes*, **9**, 7–16.
- , and J. Riser, 1981: Holocene lake deposits and paleoenvironment in central Sahara, northeastern Mali. *Palaeogeogr., Palaeoclimatol., Palaeoecol.*, **35**, 45–61.
- , and S. Kröppelin, 1991: Les climats holocènes du Sahara le long du Tropique du Cancer. *Paléoenvironnements du Sahara. Lacs Holocènes à Taoudenni (Mali)* (in French), N. Petit-Maire, Ed., Editions du CNRS, 205–210.
- , J. Fabre, P. Carbonel, E. Schulz, and A.-M. Aucour, 1987: La dépression de Taoudenni (Sahara malien) à l'Holocène (in French). *Géodynamique*, **2**, 154–160.
- , J. Riser, J. Fabre, M. Decoubert, J. Marchand, and B. Rond, 1988: *Le Sahara à l'Holocène: Mali 1:1,000,000* (in French). Institut Géographique National.
- , N. Page, and J. Marchand, 1993: *Le Sahara à l'Holocène 1:5,000,000* (in French). Laboratoire de Géologie du Quaternaire.
- Pias, J., 1970: Les formations sédimentaires tertiaires et quaternaires de la cuvette Tchadienne et les sols qui en dérivent. *Mém. ORSTOM* (in French), **43**, 408 pp.
- Pitman, A. J., 1991: A simple parameterization of sub-grid scale open water for climate models. *Climate Dyn.*, **6**, 99–112.
- Pollard, D., and S. L. Thompson, 1995: Use of a land-surface-transfer scheme (LSX) in a global climate model (GENESIS): The response to doubling stomatal resistance. *Global Planet. Change*, **10**, 129–161.
- Rand McNally, 1989: *The New International Atlas*. Rand McNally, 543 pp.

- Schneider, J. L., 1967: Evolution du dernier lacustre et peuplements préhistoriques aux bas-pays du Tchad (in French). *Bull. ASE-QUA*, 18–23.
- Servant, M., and S. Servant-Vildary, 1980: L'environnement quaternaire du bassin du Tchad. *The Sahara and the Nile: Quaternary Environments and Prehistoric Occupation in Northern Africa* (in French), A. Martin, J. Williams, and H. Faure, Eds., Balkema, 133–162.
- Snyder, C. T., and W. B. Langbein, 1962: The Pleistocene lake in Spring Valley, Nevada, and its climatic implications. *J. Geophys. Res.*, **67**, 2385–2394.
- Street, F. A., 1979: Late Quaternary precipitation estimates for the Ziway–Shala Basin, southern Ethiopia. *Palaeoecol. Africa*, **11**, 135–143.
- , 1980: The relative importance of climate and hydrogeological factors in influencing lake-level fluctuations. *Palaeoecol. Africa*, **12**, 137–158.
- , and A. T. Grove, 1976: Environmental and climatic implications of late Quaternary lake-level fluctuations in Africa. *Nature*, **261**, 385–390.
- , and —, 1979: Global maps of lake-level fluctuations since 30,000 yr B.P. *Quat. Res.*, **12**, 83–118.
- Street-Perrott, F. A., and N. Roberts, 1983: Fluctuations in closed-basin lakes as an indicator of past atmospheric circulation patterns. *Variations in the Global Water Budget*, F. A. Street-Perrott, M. Beran, and R. Ratcliffe, Eds., D. Reidel, 331–345.
- , and S. P. Harrison, 1985: Lake levels and climate reconstruction. *Paleoclimate Analysis and Modeling*, A. Hecht, Ed., Wiley, 291–340.
- , and R. A. Perrott, 1993: Holocene vegetation, lake levels and climates of Africa. *Global Climates Since the Last Glacial Maximum*, H. E. Wright Jr., J. E. Kutzbach, P. J. T. Webb III, F. A. Street-Perrott, W. F. Ruddiman, and P. J. Bartlein, Eds., University of Minnesota Press, 318–356.
- , J. F. B. Mitchell, D. S. Marchand, and J. S. Brunner, 1990: Milankovitch and albedo forcing of the tropical monsoon: A comparison of geological evidence and numerical simulations for 9000 yBP. *Trans. Roy. Soc. Edinburgh: Earth Sci.*, **81**, 407–427.
- Szesztay, K., 1974: Water balance and water level fluctuations of lakes. *Int. Assoc. Hydrol. Sci. Bull.*, **19**, 73–84.
- Tetzlaff, G., and L. J. Adams, 1983: Present-day and early-Holocene evaporation of Lake Chad. *Variations in the Global Water Budget*, F. A. Street-Perrott, M. Beran, and R. Ratcliffe, Eds., D. Reidel, 347–360.
- Thompson, S. L., and D. Pollard, 1995: A global climate model (GENESIS) with a land-surface transfer scheme (LSX). Part I: Present climate simulation. *J. Climate*, **8**, 732–761.
- UNESCO, 1978: *World Water Balance and Water Resources of the Earth*. V. I. Korzun et al., Eds., UNESCO, 663 pp.
- Vörösmarty, C. J., and B. Moore III, 1991: Modeling basin-scale hydrology in support of physical climate and global biogeochemical studies: An example using the Zambezi River. *Surv. Geophys.*, **12**, 271–311.
- , —, A. L. Grace, P. Gildea, J. M. Melillo, B. J. Peterson, E. B. Rastetter, and P. A. Steudler, 1989: Continental scale models of water balance and fluvial transport: An application to South America. *Global Biogeochem. Cycles*, **3**, 241–265.
- , —, —, B. J. Peterson, E. B. Rastetter, and J. M. Melillo, 1991: Distributed parameter models to analyze the impact of human disturbance of the surface hydrology of a large tropical drainage basin in southern Africa. *Proc. of Symp. on Hydrology for Water Management of Large River Basins*, Vienna, Austria, IAHS, 233–244.
- Wallace, J. M., and P. V. Hobbs, 1977: *Atmospheric Science an Introductory Survey*. Academic Press, 467 pp.
- World WeatherDisc, 1994: Worldwide airfield summaries. *World WeatherDisc*, WeatherDisc Associates.